High-Resolution Faraday Rotation and Electron-Phonon Coupling in Surface States of the Bulk-Insulating Topological Insulator $Cu_{0.02}Bi_2Se_3$

Liang Wu,[1,*] Wang-Kong Tse,[2,3] M. Brahlek,[4,†] C. M. Morris,[1] R. Valdés Aguilar,[1,5]
N. Koirala,[4] S. Oh,[4] and N. P. Armitage[1,‡]
[1]The Institute for Quantum Matter, Department of Physics and Astronomy, The Johns Hopkins University, Baltimore, Maryland 21218, USA
[2]Theoretical Division, Los Alamos National Laboratory, Los Alamos, New Mexico 87545, USA
[3]Department of Physics and Astronomy, MINT Center, University of Alabama, Tuscaloosa, Alabama 35487, USA
[4]Department of Physics and Astronomy, Rutgers the State University of New Jersey, New Jersey, Piscataway 08854, USA
[5]Department of Physics, The Ohio State University, Columbus, Ohio 43210, USA
(Received 15 February 2015; published 16 November 2015)

We have utilized time-domain magnetoterahertz spectroscopy to investigate the low-frequency optical response of the topological insulator $Cu_{0.02}Bi_2Se_3$ and Bi_2Se_3 films. With both field and frequency dependence, such experiments give sufficient information to measure the mobility and carrier density of multiple conduction channels simultaneously. We observe sharp cyclotron resonances (CRs) in both materials. The small amount of Cu incorporated into the $Cu_{0.02}Bi_2Se_3$ induces a true bulk insulator with only a *single* type of conduction with a total sheet carrier density of $\sim 4.9 \times 10^{12}/\mathrm{cm}^2$ and mobility as high as $4000\ \mathrm{cm}^2/\mathrm{V}\cdot\mathrm{s}$. This is consistent with conduction from two virtually identical topological surface states (TSSs) on the top and bottom of the film with a chemical potential $\sim$145 meV above the Dirac point and in the bulk gap. The CR broadens at high fields, an effect that we attribute to an electron-phonon interaction. This assignment is supported by an extended Drude model analysis of the zero-field Drude conductance. In contrast, in normal Bi_2Se_3 films, two conduction channels were observed, and we developed a self-consistent analysis method to distinguish the dominant TSSs and coexisting trivial bulk or two-dimensional electron gas states. Our high-resolution Faraday rotation spectroscopy on $Cu_{0.02}Bi_2Se_3$ paves the way for the observation of quantized Faraday rotation under experimentally achievable conditions to push the chemical potential in the lowest Landau level.

DOI: 10.1103/PhysRevLett.115.217602 PACS numbers: 76.40.+b, 72.10.Di, 78.20.Ls, 78.66.Db

Topological insulators (TIs) are a newly discovered class of materials characterized by an inverted band structure [1,2] caused by strong spin-orbit coupling. In the ideal case, they have an insulating bulk and only conduct via topologically protected massless Dirac topological surface states (TSSs). Spin-momentum locking in their electronic structure makes TIs promising platforms for spintronics applications [3]. Progress in this field has been hampered by the fact that all discovered TIs to date are slightly doped and have a conducting bulk. For instance, the proposed topological magnetoelectric effect [4] and quantized Faraday rotation [5] remain unobserved. Tuning the chemical potential towards the Dirac point and enhancing mobility were shown to be very successful in probing many-body interactions with plasmons and phonons in graphene [6], and similar advancements are expected in TIs but have not yet been realized.

The band structure of Bi_2Se_3 is one of the simplest of the 3D TIs with only a single Dirac cone at the center of the Brillouin zone. Unfortunately, native-grown Bi_2Se_3 is known to have a conducting bulk due to defects from the growth. Suppression of the bulk carrier density has been achieved by chemical-doping methods [7,8]. Nevertheless, these samples still have significant densities of bulk carriers or impurity states that are pinned near E_F. Recently, it was found that $\sim$2% Cu doping in thin films suppresses the bulk carriers and allows a true insulating state to be realized [9]. Here we investigate these copper-doped bulk insulating thin films and their decoupled TSSs [9] via magnetoterahertz spectroscopy. These films were capped by a thin insulating amorphous Se layer. Details of the growth can be found in Supplemental Material Sec. I [10] and in Ref. [9].

Cyclotron resonance (CR) experiments using terahertz spectroscopy are a powerful tool to study Dirac fermions and probe many-body interactions [21,22]. CR is also one of the most accurate measures of effective mass [23]. In previous work, a large Kerr rotation in bulk-conducting Bi_2Se_3 films was reported, but no obvious resonance was observed [24]. Cyclotron resonance has been reported in In_2Se_3 capped films [25], but the current understanding is that significant indium diffusion from In_2Se_3 to Bi_2Se_3 [26] destroys the simple non-TI–TI boundary at the interface, as a topological phase transition occurs at low indium concentrations ($\sim$6%) [27].

In the present work, we used time-domain magnetoterahertz spectroscopy with the polarization modulation technique [28] (0.5 mrad resolution; see Supplemental Material

Sec. I for experimental details [10]) to observe sharp cyclotron resonances in Faraday rotations from both $Cu_{0.02}Bi_2Se_3$ and pure Bi_2Se_3 thin films. We demonstrate that $Cu_{0.02}Bi_2Se_3$ can be described by a *single* Drude component with total carrier density $n_{2D} \sim 4.9 \times 10^{12}/\mathrm{cm}^2$. This Drude contribution is consistent with pure surface state transport with an $E_F \sim 145$ meV above the Dirac point (75 meV below the conduction band edge), which makes $Cu_{0.02}Bi_2Se_3$ a true topological insulator. CR broadening at a high field is attributed to an electron-phonon interaction. In contrast, we find two-channel conduction in pure Bi_2Se_3 films. We determine that the large Faraday rotation is induced by a dominant high-mobility TSS channel with an $E_F \sim 350$ meV. However, a weaker low-mobility second Drude term is also required to fit the data. This subdominant term most likely derives from trivial states (bulk and/or 2DEG).

In Fig. 1(a), we compare the zero-field terahertz conductance of a 64 QL $Cu_{0.02}Bi_2Se_3$ film to a pure 64 QL Bi_2Se_3 film. The Cu incorporated sample's spectra are characterized by a reduced total spectral weight and slightly lower scattering rate than the pure Bi_2Se_3. The spectra can be well fit by an oscillator model with only a Drude term describing free electronlike motion, a Drude-Lorentz term modeling the phonon, and a lattice polarizability ϵ_∞ term that originates from absorptions above the measured spectral range:

$$G(\omega) = \epsilon_0 d\left(-\frac{\omega_{pD}^2}{i\omega - \Gamma_D} - \frac{i\omega\omega_{pDL}^2}{\omega_{DL}^2 - \omega^2 - i\omega\Gamma_{DL}} - i(\epsilon_\infty - 1)\omega\right). \tag{1}$$

Here Γ's are scattering rates, ω_p's are plasma frequencies, and d is the film thickness. The spectral weight $(\omega_{pD}^2 d)$ is proportional to the integrated area of each feature in the real part of the conductance. It gives the ratio of carrier density to an effective transport mass:

$$\frac{2}{\pi\epsilon_0}\int G_{D1} d\omega = \omega_{pD}^2 d = \frac{n_{2D} e^2}{m^* \epsilon_0}. \tag{2}$$

Here m^* is defined as $\hbar k_F / v_F$ for "massless Dirac fermions." Considering the TSS dispersion up to quadratic corrections $E = Ak_F + Bk_F^2$, the spectral weight can be expressed in terms of k_F, where A and B are parameters obtained from ARPES (see Supplemental Material Sec. II [10]):

$$\omega_{pD}^2 d = \frac{k_F(A + 2Bk_F)e^2}{2\pi\hbar^2\epsilon_0}. \tag{3}$$

This expression assumes that the single-channel conduction originates in two nominally identical TSSs. From the spectral weight analysis, having determined k_F, we can then calculate both n_{2D} (proportional to k_F^2) and m^*. From these Drude-Lorentz fits, we find a *total* sheet carrier density $n_{2D} \sim 5.0 \times 10^{12}/\mathrm{cm}^2$, $m^* \sim 0.14 m_e$, and $E_F \sim 145(\pm 5)$ meV according to Eq. (3).

We can estimate the carrier density and mass by the zero-field spectra alone, because both can be expressed as a function of k_F. Below, we determine the mass in a model-free fashion through CR experiments. The signature of CR is a peak in the real part of the conductance [Fig. 1(b)], an inflection point in the real part of Faraday rotation θ_F' [Fig. 1(c)], and a dip in the imaginary part of Faraday rotation θ_F'' [Fig. 1(d)]. Its full width at half maximum (FWHM) is the scattering rate. Field-dependent complex Faraday rotation data are shown in Figs. 1(c) and 1(d). One can see that an edge feature around an inflection point in θ_F' and a dip in θ_F'' shifts to higher frequency with increasing field, which is consistent with CR. We fit the data by a Drude-Lorentz model accounting for the field dependence of the Drude term and constraining the parameters of the phonon and ϵ_∞ by the values extracted from the zero-field conductance fits. The conductance in a magnetic field can be described by the expression

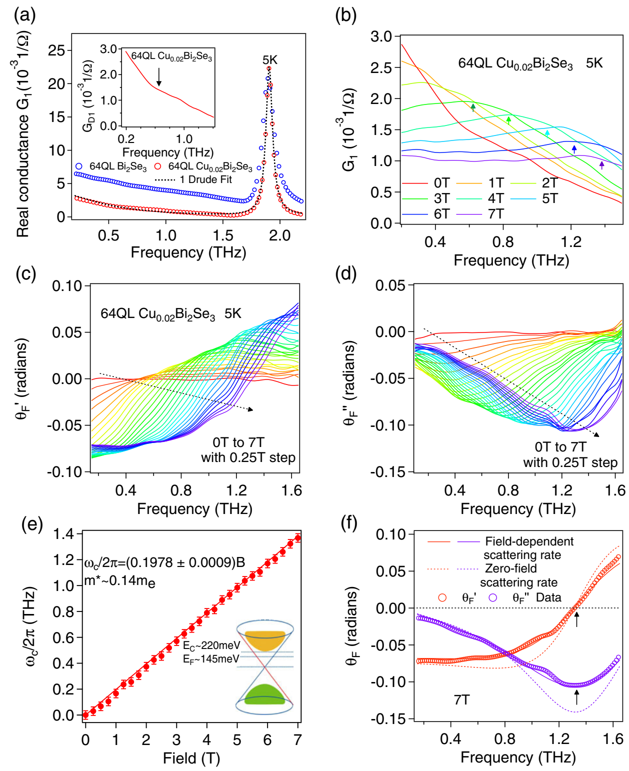

FIG. 1 (color online). Data summary for 64 quintuple layer (QL) $Cu_{0.02}Bi_2Se_3$ (sample1). (a) Real sheet conductance of 64 QL $Cu_{0.02}Bi_2Se_3$ and pure Bi_2Se_3 films at 5 K. The inset is the Drude conductance G_D of 64 QL $Cu_{0.02}Bi_2Se_3$ after subtracting the phonon and ϵ_∞ contributions. The arrow indicates the deviation from pure Lorentzian form that arises from electron-phonon coupling. (b) Field-dependent conductance at 5 K. Arrows are guides to the eye for cyclotron frequencies. (c) Real and (d) imaginary parts of the complex Faraday rotation data at different fields at 5 K. (e) Cyclotron frequency versus field. The solid line is a linear fit. The inset is a cartoon indicating $E_F \sim 145$ meV above the Dirac point (75 meV below the conduction band minimum). (f) Complex Faraday angle with fits at 7 T. The solid curve is a fit with a field-dependent scattering rate. The dashed curve is a fit using the zero-field scattering rate. Arrows are guides to the eye for cyclotron frequency.

$$G_{\pm} = -i\epsilon_0 \omega d \left(\frac{\omega_{pD}^2}{-\omega^2 - i\Gamma_D \omega \mp \omega_c \omega} + \frac{\omega_{pDL}^2}{\omega_{DL}^2 - \omega^2 - i\omega\Gamma_{DL}} + (\epsilon_\infty - 1) \right). \quad (4)$$

Here the $\pm$ sign signifies the response to right- or left-hand circularly polarized light, respectively. ω_c is the CR frequency to be defined below. The Faraday rotation can be expressed as $\tan(\theta_F) = -i(t_+ - t_-)/(t_+ + t_-)$ [29]. Note that the Faraday equation is a complex quantity, because, in addition to rotations, phase shifts that are different for right- or left-hand polarized light can be accumulated. The imaginary part is related to the ellipticity [28].

The fits to this model for the Faraday rotation are shown for a representative field of 7 T in Fig. 1(f) (see Supplemental Material Sec. II for fits to all fields [10]). In this plot, the dashed curves are from a fit with the spectral weight and scattering rate ~0.4 THz set by the zero-field conductance fit (e.g., only ω_c allowed to vary). One can see that, although the gross features of the spectra are reproduced, using the zero-field scattering rate entirety fails to reproduce certain aspects of the Faraday rotation, including the value of the minimum in θ_F''. A much better fit (solid line) can be obtained by letting the scattering rate vary with the field while keeping other parameters (except for ω_c) fixed. The origin of this field-dependent scattering rate will be addressed below. The fits allow us to extract the cyclotron frequency as a function of field; it is exhibited by the raw spectra as the minimum in θ_F''. As shown in Fig. 1(e), a linear fitting using the expected relation between the mass and the resonance frequency $\omega_c = eB/m^*$ gives an effective mass of $0.14m_e$. By using Eq. (2) and the spectral weight obtained from fitting Faraday rotation, we can extract a *total* sheet carrier density $n_{2D} = 4.9 \pm 0.1 \times 10^{12}/\text{cm}^2$. With the known band structure of Bi_2Se_3, this charge density, and the observation of a single kind of charge carrier, is consistent only with two essentially identical TSSs and an $E_F \sim 145$ meV above the Dirac point. We can conclude that $Cu_{0.02}Bi_2Se_3$ has an insulating bulk and for the sample highlighted here a high mobility $\mu = e/\Gamma_D m^* \sim 4000\ \text{cm}^2/\text{V}\cdot\text{s}$. The features were robust to sample aging, as the samples (with the amorphous Se cap) maintain bulk-insulating and high mobility after sitting in air for eight months (see Supplemental Material Sec. II [10]).

Films of $Cu_{0.02}Bi_2Se_3$ can be contrasted with films of pure Bi_2Se_3, which is known to have the surface chemical potential pinned in the bulk conduction band [30,31]. We develop a self-consistent data analysis method and use our high-resolution magnetoterahertz spectroscopy to precisely determine the contribution of the subdominant bulk. In Fig. 2(a), we show zero-field conductance spectra from a typical 100 QL Bi_2Se_3 film. It has higher spectral weight than $Cu_{0.02}Bi_2Se_3$, consistent with a higher charge density. For the same reason, the plateaulike Faraday rotation at 7 T at low frequencies in Fig. 2(f) is as large as ~0.25 rad, while the value for the $Cu_{0.02}Bi_2Se_3$ sample is ~0.07 rad.

In Figs. 2(b)–2(d), one can see that the CR is exhibited at lower frequencies, which indicates that Bi_2Se_3 has a higher CR mass. In Fig. 2(e), the linear fit of ω_c versus B gives an effective mass ~$0.20m_e$. We believe that this derives from TSSs, as this mass is inconsistent with the accepted values for the bulk bands [32] or band-bending-induced surface 2DEG bands [33]. Note that the value of the CR mass in Bi_2Se_3 we determine here is different than that given in our previous work [24]. The reason for this discrepancy is discussed at length in Supplemental Material Sec. VI [10].

One can see from Fig. 2(f) that fits of the Faraday rotation using only a single Drude term are reasonably good. As

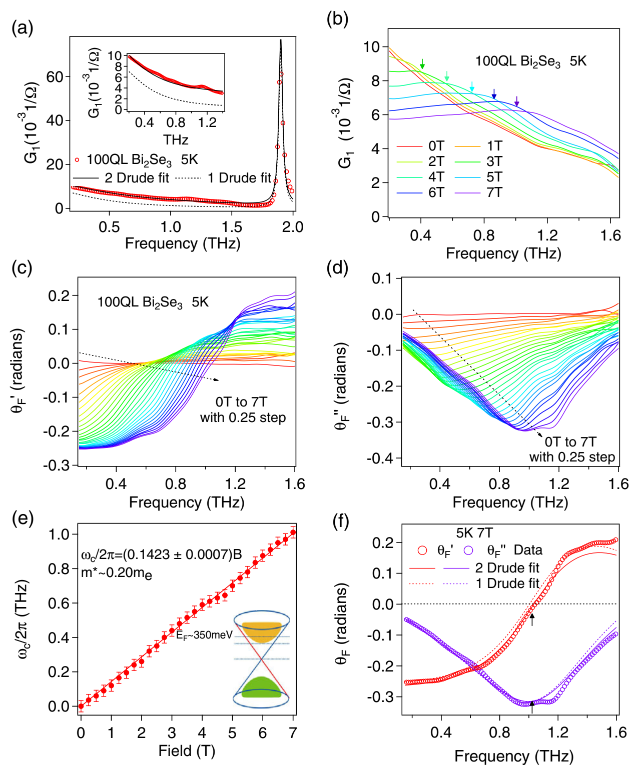

FIG. 2 (color online). (a) Real conductance of 100 QL Bi_2Se_3 comparing single- and two-component Drude fits as detailed in the text. The inset enlarges the low-frequency regime. (b) Field-dependent conductance at 5 K. (c) The real and (d) imaginary parts of the complex Faraday rotation data at different fields at 5 K. (e) The cyclotron resonance frequency versus field. The inset is a cartoon indicating $E_F \sim 350$ meV above the Dirac point. (f) Complex Faraday rotation data with one- and two-component Drude fits at 7 T. The dashed and solid curves are one- and two-Drude fits, respectively.

before, we use the spectral weight and CR mass by Eq. (2) to extract a total sheet carrier density $n_{2D} \sim 1.9 \pm 0.1 \times 10^{13}/\text{cm}^2$. This compares favorably to a density of $n_{2D} \sim 2.0 \times 10^{13}/\text{cm}^2$, a mass of $\sim 0.20 m_e$, and an $E_F \sim 350$ meV that we can determine purely from an analysis of the spectral weight using the TSS dispersion by Eq. (3). We determine a mobility of $\mu \sim 3200\ \text{cm}^2/\text{V}\cdot\text{s}$ of the TSSs.

However, while the fits to the Faraday rotation with a single Drude term are excellent, significant discrepancies arise if we use the resulting parameters to fit the conductance data. In Fig. 2(a), one can see that the single Drude component fit significantly underestimates the conductance by a roughly constant amount over the entire spectral range. As E_F is in the bottom of the conduction band, it is reasonable to ascribe this difference to a subdominant low-mobility conduction channel originating in the bulk or 2DEG. Adding a second term with a large scattering rate ($\Gamma/2\pi > 4$ THz such that the contribution to the real conductance is a constant offset) improves the conductance fit dramatically. If literature values for the bulk or 2DEG mass are used, this channel has a carrier density of $n_{2D} \sim 8.0 \times 10^{12}/\text{cm}^2$ and a low mobility of $\mu < 300\ \text{cm}^2/\text{V}\cdot\text{s}$. The second flat Drude term adds only a featureless small background to the Faraday rotation. The ratio $G_{1\text{TSS}}/G_{1\text{total}} \geq 90\%$ at low frequencies confirms that TSSs dominate transport as inferred in previous terahertz measurements [24,27].

Having identified the transport channels in these films and their relevant parameters, we can look in more detail at the magnetic field dependence of the scattering rates. As shown in Fig. 3(a), the scattering rate $\Gamma_D/2\pi$ in $Cu_{0.02}Bi_2Se_3$ increases with cyclotron frequency or field, displaying a maximum near a cyclotron frequency of 0.9 ± 0.1 THz. As discussed in Supplemental Material Sec. III [10], we can exclude magnetic-field-induced spin- or orbital-based electronic mechanisms for this broadening [34]. We plot the scattering rate versus the cyclotron frequency instead of versus the magnetic field in order to allow a direct comparison with the measurement and phonon frequencies. One can understand the magnetic field as an energy-sampling process as follows. With increasing field, the Drude peak center frequency ω_c shifts to higher energies. As the Drude peak overlaps with the phonon frequency, one expects the scattering rate to reach its maximum value and saturate, as one generally expects that the CR will become broader at frequencies above the relevant phonon frequency because new scattering channels emerge. Similar CR broadening has been observed in GaInAs quantum wells and graphene and ascribed to electron-phonon coupling [35,36].

An extended Drude model (EDM) analysis [37] of the *zero-field* Drude conductance supports the inference that the broadening is due to coupling to a low-energy mode such as a phonon. Such an analysis allows one to quantify subtle deviations from pure Drude behavior (e.g., pure Lorentzian form) as shown in the inset in Fig. 1(a) in the form of frequency-dependent mass renormalizations $m^*_{RN}(\omega)$ and scattering rates $\Gamma_D/2\pi(\omega)$ shown in Fig. 3. In such an analysis, one inverts the Drude intraband contribution to the conductance (G_D) via Eqs. (5):

$$\Gamma_D(\omega) = \frac{1}{\tau(\omega)} = \frac{\omega_{pD}^2 d}{4\pi}\text{Re}\left(\frac{1}{G_D}\right),$$
$$\frac{m^*_{RN}(\omega)}{m_b} = -\frac{\omega_{pD}^2 d}{4\pi\omega}\text{Im}\left(\frac{1}{G_D}\right). \tag{5}$$

Here m_b is the band mass without interaction renormalization. An EDM analysis shows a frequency-dependent scattering rate $\Gamma_D(\omega)$ and an electron-phonon coupling constant ($\lambda = (m^*_{RN}/m_b) - 1$) defined at the dc limit $\sim 0.55 \pm 0.05$. Since the mass renormalization here is reasonably small, we approximate the bare plasma frequency with the value extracted from zero-field conductance or CR fits.

From the EDM parameters we can define the "fully renormalized" scattering rate $\Gamma^*_D(\omega) = \Gamma_D(\omega)/[m^*_{RN}(\omega)/m_b]$, which is manifested as the actual width of the low-frequency Drude feature [e.g., the Γ_D of Eq. (4)] [38]. Plotting this quantity in Fig. 3(a), we find that the general trend and energy scales of the scattering rate from the EDM are about the same as those from the CR fit. One can see that the result from EDM is a sharper version of the curve from the CR fit, which may be expected because the CR fit assumed a frequency-independent scattering rate, and as such means it is an average over a (weakly) frequency-dependent quantity.

For the first time, we have demonstrated a correspondence between the spectral features in a CR experiment and EDM analyses, which indicates that the magnetic field itself is not the source of the CR broadening. We propose electron-phonon coupling as the cause of these effects [39–42], as the energy scale of the threshold in the

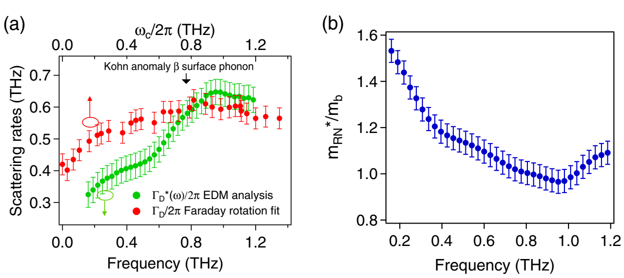

FIG. 3 (color online). (a) The scattering rate as a function of cyclotron frequency (red). The fully renormalized scattering rate by mass through extended Drude analysis as a function of frequency (green). The black arrow indicates β surface phonon frequency at the Kohn anomaly. (b) The renormalized mass as a function of frequency. The error bars express the uncertainty in ω_{pD}.

scattering rate matches that of a number of electron-phonon scales in this system. The value is close to the scale of the previously observed Kohn anomaly of the surface β phonon, 0.75 THz at $2k_F$ [40,43]. It also matches closely the scale of the maximum acoustic phonon energy that can couple to cross Fermi surface scattering $c \times 2k_F/2\pi$ $\sim$0.6 THz (where c is the acoustic phonon velocity) [41]. The coupling strength λ extracted by EDM is close to the value $\lambda \sim 0.43$ by analysis of the Kohn anomaly [44] and also agrees with the calculation $\lambda \sim 0.42$ for acoustic phonons in thin film geometry [42]. The coupling constant we observed is within the different values ARPES gives [45–47]. The energy scale of the 3 meV mode found via ARPES in Ref. [47] agrees well with the characteristic energy here. The lower coupling strength we observed may be due to the lower chemical potential of our sample than that used in Ref. [47].

Looking forward, our results demonstrate the possibility of observing a quantized Faraday rotation in such films of a TI. For the quantized Faraday rotation of a film on a substrate, one has $\tan(\theta_F) = 2\alpha/(1+n)(\nu + 1/2) \sim$ 3.5 mrad$(\nu + 1/2)$ for each surface state in the quantum regime, where α is the fine structure constant, ν is the filling factor, and n is the substrate index of refraction. The Landau level spectrum will be $E(\pm\nu) = \pm v_F\sqrt{2e\hbar B|\nu|}$. In order to reach the lowest Landau level in this true topological insulator $Cu_{0.02}Bi_2Se_3$ will require 150 T, which may be achievable for future terahertz experiments at pulse field facilities. Electric field gating the present samples in a terahertz-compatible arrangement would bring down this field threshold. We hope our high-resolution Faraday rotation spectroscopy will enable the observation of the long-sought quantized Faraday rotation and topological magnetoelectric effect [4,5].

We thank A. Kuzmenko, G. Refael, and S. Valenzuela for discussions and L. Pan for assistance with the figures. Terahertz measurements at JHU and film growth and development at Rutgers were supported by NSF DMR-1308142, with additional support by the Gordon and Betty Moore Foundation through Grant No. GBMF2628 to N. P. A. at JHU and EPiQS Initiative Grant GBMF4418 to S. O. at Rutgers and by ONR-N000141210456 at Rutgers. Work at Los Alamos National Laboratory (LANL) was carried out under the auspices of the U.S. Department of Energy at LANL under Contract No. DE-AC52-06NA25396.

[*]lwu29@jhu.edu
[†]Present address: Department of Materials Science and Engineering, Pennsylvania State University, University Park, PA 16801, USA.
[‡]npa@jhu.edu

[1] M. Z. Hasan and C. L. Kane, Rev. Mod. Phys. **82**, 3045 (2010).
[2] X.-L. Qi and S.-C. Zhang, Rev. Mod. Phys. **83**, 1057 (2011).
[3] D. Pesin and A. H. MacDonald, Nat. Mater. **11**, 409 (2012).
[4] X.-L. Qi, T. L. Hughes, and S.-C. Zhang, Phys. Rev. B **78**, 195424 (2008).
[5] W.-K. Tse and A. H. MacDonald, Phys. Rev. Lett. **105**, 057401 (2010).
[6] D. Basov, M. Fogler, A. Lanzara, F. Wang, and Y. Zhang, Rev. Mod. Phys. **86**, 959 (2014).
[7] Z. Ren, A. A. Taskin, S. Sasaki, K. Segawa, and Y. Ando, Phys. Rev. B **82**, 241306 (2010).
[8] J. Xiong, A. Petersen, D. Qu, Y. Hor, R. Cava, and N. Ong, Physica (Amsterdam) **44E**, 917 (2012).
[9] M. Brahlek, N. Koirala, M. Salehi, N. Bansal, and S. Oh, Phys. Rev. Lett. **113**, 026801 (2014).
[10] See Supplemental Material at http://link.aps.org/supplemental/10.1103/PhysRevLett.115.217602 Experimental methods, more data and discussion on $Cu_{0.02}Bi_2Se_3$ and Bi_2Se_3, calculations about transport lifetime of the topological insulators in external magnetic fields, effects of Se and In_2Se_3 capping, discussions on one-Drude-component and two-Drude-component fits, role of copper and band bending, which includes Refs. [11–20].
[11] R. Valdés Aguilar, L. Wu, A. V. Stier, L. S. Bilbro, M. Brahlek, N. Bansal, S. Oh, and N. P. Armitage, J. Appl. Phys. **113**, 153702 (2013).
[12] L. Wu, M. Brahlek, R. V. Aguilar, A. V. Stier, C. M. Morris, Y. Lubashevsky, L. S. Bilbro, N. Bansal, S. Oh, and N. P. Armitage, Nat. Phys. **9**, 410 (2013), supplementary information.
[13] Y. Cao *et al.*, Nat. Phys. **9**, 499 (2013).
[14] Y. Zhang *et al.*, Nat. Phys. **6**, 584 (2010).
[15] C. H. Yang, F. M. Peeters, and W. Xu, Phys. Rev. B **82**, 075401 (2010).
[16] O. E. Raichev and F. T. Vasko, *Quantum Kinetic Theory and Applications* (Springer, New York, 2005).
[17] D. Culcer and S. Das Sarma, Phys. Rev. B **83**, 245441 (2011); D. Culcer, E. H. Hwang, T. D. Stanescu, and S. Das Sarma, Phys. Rev. B **82**, 155457 (2010).
[18] T. Ando and Y. Uemura, J. Phys. Soc. Jpn. **36**, 959 (1974); T. Ando, J. Phys. Soc. Jpn. **36**, 1521 (1974); **37**, 622 (1974); **37**, 1233 (1974).
[19] N. H. Shon and T. Ando, J. Phys. Soc. Jpn. **67**, 2421 (1998); Y. Zheng and T. Ando, Phys. Rev. B **65**, 245420 (2002).
[20] I. Dmitriev, A. Mirlin, D. Polyakov, and M. Zudov, Rev. Mod. Phys. **84**, 1709 (2012).
[21] I. Crassee, J. Levallois, A. Walter, M. Ostler, A. Bostwick, E. Rotenberg, T. Seyller, D. Van Der Marel, and A. Kuzmenko, Nat. Phys. **7**, 48 (2011).
[22] Z. Jiang, E. A. Henriksen, L. C. Tung, Y.-J. Wang, M. E. Schwartz, M. Y. Han, P. Kim, and H. L. Stormer, Phys. Rev. Lett. **98**, 197403 (2007).
[23] J. Kono and N. Miura, *High Magnetic Fields: Science and Technology* (World Scientific, Singapore, 2006), Vol. III.
[24] R. Valdés Aguilar *et al.*, Phys. Rev. Lett. **108**, 087403 (2012).
[25] G. S. Jenkins, D. C. Schmadel, A. B. Sushkov, H. D. Drew, M. Bichler, G. Koblmueller, M. Brahlek, N. Bansal, and S. Oh, Phys. Rev. B **87**, 155126 (2013).
[26] H. Lee, C. Xu, S. Shubeita, M. Brahlek, N. Koirala, S. Oh, and T. Gustafsson, Thin Solid Films **556**, 322 (2014).

[27] L. Wu, M. Brahlek, R. V. Aguilar, A. V. Stier, C. M. Morris, Y. Lubashevsky, L. S. Bilbro, N. Bansal, S. Oh, and N. P. Armitage, Nat. Phys. **9**, 410 (2013).

[28] C. Morris, R. Valdés Aguilar, A. Stier, and N. Armitage, Opt. Express **20**, 12303 (2012).

[29] The transmission can be analyzed according to the thin film transmission equation for each polarization handedness separately. $t_\pm$ is the transmission for right- or left-hand circularly polarized light. $t_\pm = t_{vs}e^{i\phi_s}t_{sfv\pm}$ is the transmission for right- or left-hand circularly polarized light, where t_{vs} is the transmission from vacuum to substrate $t_{vs} = 2/(1+n_s)$ and $t_{sfv\pm}$ is the transmission from the substrate though film and then to vacuum $t_{sfv\pm} = 2n_s/(1+n_s+Z_0G_\pm)$. $e^{i\phi_s}$ is the phase accumulation inside the substrate [48].

[30] Y. Xia *et al.*, Nat. Phys. **5**, 398 (2009).

[31] N. Bansal, Y. S. Kim, M. Brahlek, E. Edrey, and S. Oh, Phys. Rev. Lett. **109**, 116804 (2012).

[32] H. Hohler, Phys. Status Solidi (b) **58**, 91 (1973).

[33] M. Bianchi, D. Guan, S. Bao, J. Mi, B. B. Iversen, P. D. C. King, and P. Hofmann, Nat. Commun. **1**, 128 (2010).

[34] In principle, the Zeeman effect and orbital effect should increase the scattering rate as well. Nevertheless, the Zeeman effect should be much smaller than a 50% increase at low field. Orbital effects will lead to magneto-oscillations of transport lifetime (inverse scattering rate) above 3 T when $\omega_c\tau \geq 1$. (See Supplemental Material Sec. III for a detailed calculation.)

[35] M. Orlita, C. Faugeras, G. Martinez, S. A. Studenikin, and P. J. Poole, Europhys. Lett. **92**, 37002 (2010).

[36] M. Orlita, L. Z. Tan, M. Potemski, M. Sprinkle, C. Berger, W. A. de Heer, S. G. Louie, and G. Martinez, Phys. Rev. Lett. **108**, 247401 (2012).

[37] J. W. Allen and J. C. Mikkelsen, Phys. Rev. B **15**, 2952 (1977).

[38] $\Gamma_D^*(\omega)$ includes the renormalization effects of the lifetime as well as the mass. $\Gamma_D^*(\omega) = \{[\Gamma_D(\omega)]/[m_{RN}^*(\omega)/m_b]\} = \omega[\mathrm{Re}(G_D)/\mathrm{Im}(G_D)]$, which tells us the frequency-dependent scattering rate. Note that $\Gamma_D^*(\omega)$ does not depend on the plasma frequency.

[39] J. A. Sobota, S.-L. Yang, D. Leuenberger, A. F. Kemper, J. G. Analytis, I. R. Fisher, P. S. Kirchmann, T. P. Devereaux, and Z.-X. Shen, Phys. Rev. Lett. **113**, 157401 (2014).

[40] X. Zhu, L. Santos, R. Sankar, S. Chikara, C. Howard, F. C. Chou, C. Chamon, and M. El-Batanouny, Phys. Rev. Lett. **107**, 186102 (2011).

[41] D. Kim, Q. Li, P. Syers, N. P. Butch, J. Paglione, S. D. Sarma, and M. S. Fuhrer, Phys. Rev. Lett. **109**, 166801 (2012).

[42] S. Giraud, A. Kundu, and R. Egger, Phys. Rev. B **85**, 035441 (2012).

[43] Reference [40] reported the surface β phonon has a frequency of ∼1.8 THz and the surface spring constant is 75% of the bulk value. Therefore, the surface β phonon could be a softening bulk A_{1g} Raman active phonon (2.23 THz bulk value). The surface β phonon shows a Kohn anomaly at $2k_f$ with ∼0.75 THz phonon frequency.

[44] Xuetao Zhu, L. Santos, C. Howard, R. Sankar, F. C. Chou, C. Chamon, and M. El-Batanouny, Phys. Rev. Lett. **108**, 185501 (2012).

[45] R. C. Hatch, M. Bianchi, D. Guan, S. Bao, J. Mi, B. B. Iversen, L. Nilsson, L. Hornekær, and P. Hofmann, Phys. Rev. B **83**, 241303 (2011).

[46] Z.-H. Pan, A. V. Fedorov, D. Gardner, Y. S. Lee, S. Chu, and T. Valla, Phys. Rev. Lett. **108**, 187001 (2012).

[47] T. Kondo *et al.*, Phys. Rev. Lett. **110**, 217601 (2013).

[48] J. N. Hancock, J. L. M. van Mechelen, A. B. Kuzmenko, D. van der Marel, C. Brüne, E. G. Novik, G. V. Astakhov, H. Buhmann, and L. W. Molenkamp, Phys. Rev. Lett. **107**, 136803 (2011).